ISSN: 2639-7455

Research Article

Earth & Environmental Science Research & Reviews

From Behavioral Climate Models and Millennial Data to AGW Reassessment

Philippe de Larminat

University Professor Institut de Recherche en Communication et Cybernétique de Nantes (IRCCyN), now LS2N (Nantes, France).

Corresponding Author

Philippe de Larminat, Institut de Recherche en Communication et Cybernétique de Nantes (IRCCyN), now LS2N (Nantes, France).

Submitted: 02 Feb 2023; **Accepted**: 22 Feb 2023; **Published**: 16 Mar 2023

Citation: Larminat, P. De., (2023). From Behavioral Climate Models and Millennial Data to AGW Reassessment. *Eart & Envi Scie Res & Rev, 6*(2), 410-424.

Abstract

Context. The so called AGW (Anthropogenic Global Warming), is based on thousands of climate simulations that indicate that human activity is virtually solely responsible for the recent global warming. The climate models used are derived from the meteorological models used for short-term predictions. They are based on the fundamental and empirical physical laws that govern the myriad of atmospheric and oceanic cells integrated by the finite element technique. Numerical approximations, empiricism and the inherent chaos in fluid circulations make these models questionable for validating the anthropogenic principle, given the accuracy required (better than one per thousand) in determining the Earth energy balance.

Aims and methods. *The purpose is to quantify and simulate behavioral models of weak complexity, without referring to predefined parameters of the underlying physical laws, but relying exclusively on generally accepted historical and paleoclimate series.*

Results. *These models perform global temperature simulations that are consistent with those from the more complex physical models. However, the repartition of contributions in the present warming depends strongly on the retained temperature reconstructions, in particular the magnitudes of the Medieval Warm Period and the Little Ice Age. It also depends on the level of the solar activity series. It results from these observations and climate reconstructions that the anthropogenic principle only holds for climate profiles assuming almost no PCA neither significant variations in solar activity. Otherwise, it reduces to a weak principle where global warming is not only the result of human activity, but is largely due to solar activity.*

Keywords: *AGW Assessment; Reduced Complexity Models; Parameter Identification; Millennial Climate Series*

Introduction

The IPCC (Intergovernmental Panel on Climate Change) defines its mission in *"Principles Governing IPCC Work"*, as *"to assess […] the scientific basis of risk of human-induced climate change"*. In agreement with this mission, the anthropogenic principle is corroborated by a large amount of climate simulations concluding that the current warming results from human activity alone. Most of them come from the *Coupled Model Intercomparison Projects* (CMIPs), organized by the *Working Group on Coupled Modelling of the World Climate Research Program* and are synthesized through Figure 1-b of the Summary for Policymakers (SPM) of AR6 (Assessment Report 6) of [1].

GCMs (short acronym for AOCGM: Atmosphere Ocean General Circulation Models, or for Global Climate model) are fed by series related to *climate drivers*. Some are of human origin: fossil fuel combustion, industrial aerosols, changes in land use, condensation trails, etc. Others are of natural origin: solar and volcanic activities, Earth's orbital parameters, geomagnetism, internal variability generated by atmospheric and oceanic chaos. These drivers, or *forcing factors*, are expressed in their own units: total solar irradiance ($W\ m^{-2}$), atmospheric concentrations of GHG (*ppm*), optical depth of industrial or volcanic aerosols (*dimless*), oceanic indexes (ENSO, AMO...), or by annual growth rates (%). Climate scientists have introduced a metric in order to characterize the relative impact of the different climate drivers on climate change. This metric is that of radiative forcings (RF), designed to quantify climate drivers through their effects on the terrestrial radiation budget at the top of the atmosphere (TOA).

Knowing that all 'physical' climate models, simple or complex, respect the fundamental law of conservation of energy, the distribution of the contributions will necessarily closely reproduce that of the radiative forcings, e.g. a ratio of about one-to-ten between the powers attributed to solar and anthropogenic forcing (see Fig. 3 further). However, independently of the physical units and associated energy properties of the RFs, one can recognize their signatures in the output and deduce their contributions. For example, volcanic eruptions are identifiable events whose contributions can be quantified without reference to either their assumed radiative forcings, or to physical modeling of aerosol diffusion in the atmosphere. Similarly, the *Preindustrial Climate Anomalies* (PCA) gathering the Medieval Warm Period (MWP) and the Little Ice Age (LIA), shows a profile similar to that of the solar forcing reconstructions. Per the methodology proposed in this paper, the respective contributions of the RF inputs are quantified through *behavior models, or black-box models.* Section 2 presents and compares the temperature series coming from databases quoted in IPCC reports. In Section 3, the concept of radiative forcing is discussed. Forcings include not only anthropogenic, solar and volcanic forcings, referred to as "external" forcings, but also oceanic indexes (e.g. El Niño), and understood as "internal" forcings. Section 4 develops a behavior model limited to second order transfer functions, equivalent to the equations of a two-layer model (details in appendix). These models incorporate possible multiplicative scaling factors on the assumed radiative forcing data.

The *identification* principles are presented in section 5. Parameters are estimated by linear regressions from the global mean surface temperature (GMST). The ocean heat content measurement defines a second set of data enabling the evaluation of the terrestrial climate feedback coefficient, as well as the scaling factors to be applied to the given radiative forcings series.

Now, Figures 1-a and 1-b presents simulations obtained from the models identified under two different sets of assumptions, detailed in sections 6 and 7 respectively.

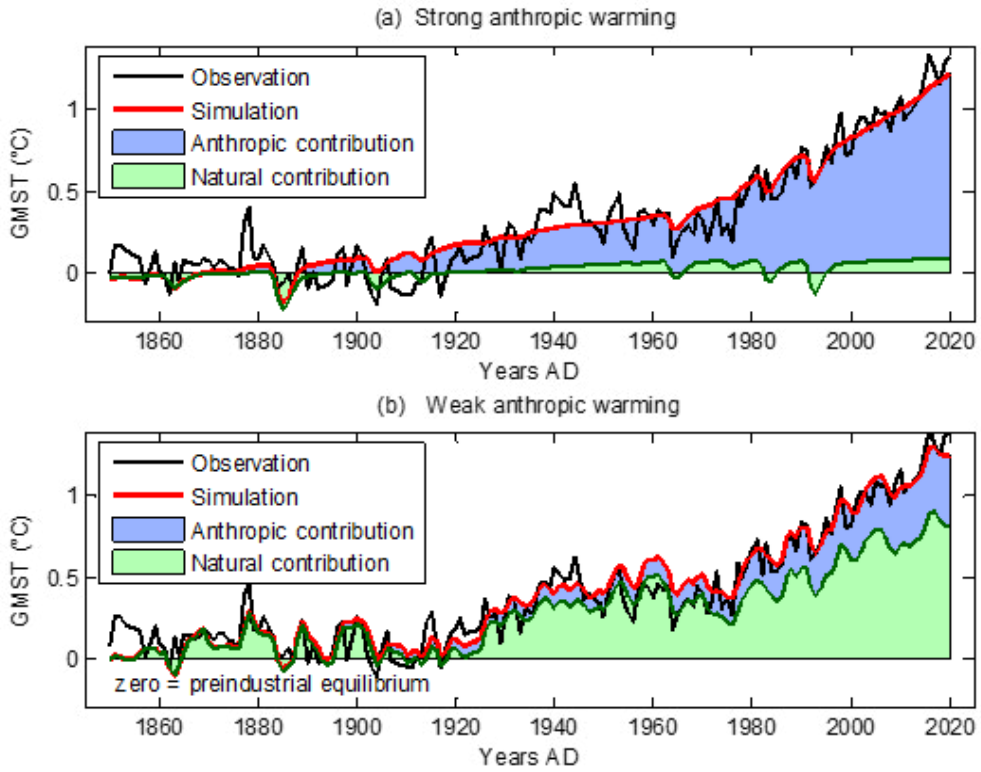

Figure 1. Anthropgenic and natural contributions. (a) Locked scaling factors, weak PCA. (b) Free scaling, strong PCA

In both cases, the overall result for the global temperature simulation (red) fits fairly well with the observations (black). Curves also show the forcing contributions to modern warming (since 1850). From this perspective, the natural (green) and anthropogenic (blue) contributions are in strong contradiction between panels (a) and (b). This incompatibility is at the heart of our work. Simulations in panel (a) are calculated per section 6, where the scaling multipliers planned in the model are locked to unity, so that the radiative forcing inputs are constrained to strictly comply with the IPCC quantification. The remaining parameters of the black-box model are adjusted in order to minimize the deviation between the observations (black curve) and the simulated outputs (red). Per these assumptions, the resulting contributions (blue vs. green) comply with the AGW principle. Also, the conformity of the results with those of the CMIP supports the validity of the type of behavioral model adopted for our simulations.

In section 7, the scaling factors are unlocked, which allows quantifying possible over- or underestimations of the given radiative forcing series. The results depend on the temperatures and solar activity data selected for the model fitting, in particular during the pre-industrial period (850-1850). In the assumption of a high PCA, the results on the respective contributions are completely turned upside down; the natural contribution to warming becomes predominant (Fig. 1-b), and the estimated scaling factors reflect a strong overestimation of anthropogenic forcings, and a corresponding underestimation of solar forcing. Section 7 discusses the plausibility of this anthropogenic scaling and Section 8 shows that highly variable solar activity reconstructions are needed to replicate strong PCA. Section 9 concludes that the level of pre-industrial temperatures as well as the solar forcings plays a key role in determining human and natural contributions to current climate warming.

Paleoclimate Temperatures

Although historically documented the Medieval Warm Period (MWP) and the Little Ice Age (LIA) don't make consensus about their amplitudes and geographic extensions [2, 3]. In Fig. 7.1-c of the First Assessment Report of IPCC, a reconstruction from showed a peak PCA amplitude of about 1.2 °C [4]. The later on, a reconstruction by the so-called *'hockey stick graph'*, was reproduced five times in the IPCC Third Assessment Report (2001), wherein there was no longer any significant MWP [5]. After, R. 2003 controversies reference to this reconstruction had disappeared from subsequent IPCC reports: it is not included among the fifteen paleoclimate reconstructions covering the millennium period listed in the fifth report (AR5, 2013) [6]. Nevertheless, AR6 (2021) revived a hockey stick graph reconstruction from a consortium initiated by a network "PAst climate chanGES" [7,8]. The IPCC assures (AR6, 2.3.1.1.2): *"this synthesis is generally in agreement with the AR5 assessment"*. Figure 2 below puts this claim into perspective. It shows the fifteen reconstructions covering the pre-industrial period accredited by the IPCC in AR5 (2013, Fig. 5.7 to 5.9, and table 5.A.6), compiled (Pangaea database) by [7]. Visibly, the claimed agreement of the PAGES2k reconstruction (blue) with the AR5 green lines does not hold.

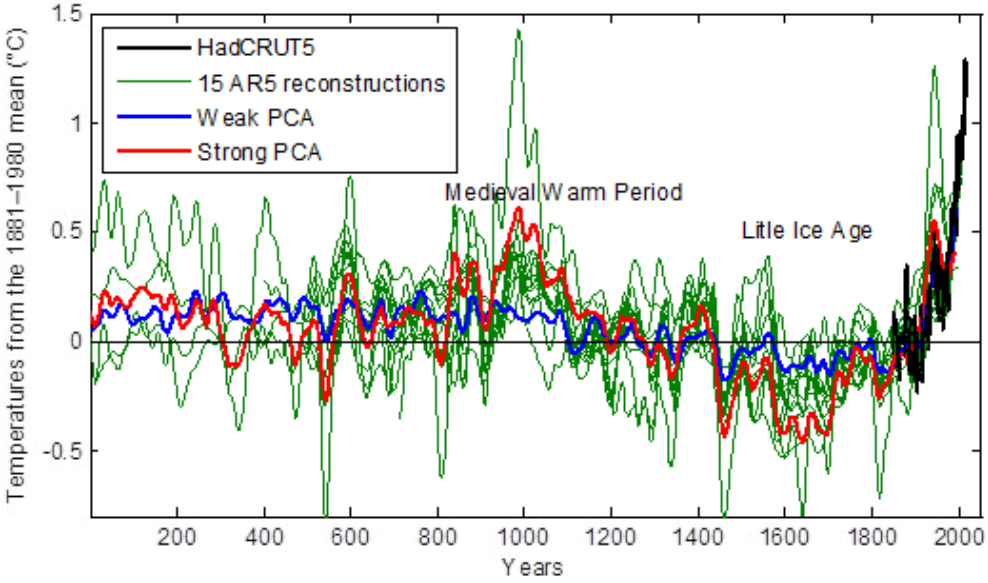

Figure 2. Weak ant strong preindustrial climate anomaliess, respectively from AR5 (2013) and AR6 (2021).

The purpose of this paper is not to discuss the PCA level in itself, but to analyze its potential impact on the validation of the anthropogenic principle. To this end, we consider on the one hand the weak PCA defined as PAGES2k (blue); on the other hand a strong PCA (red) defined as the average of the four AR5 reconstructions that show the highest PCA: [9-12]. This deliberated data picking is intended to highlight the importance of paleoclimate reconstructions in assessing the contributions to current warming, without prejudging their respective relevance.

Climate forcings

We first distinguish between *external forcings,* which lead to the *radiative forcings* in the usual sense, resulting from the external imbalance factors, and the *internal forcings*, associated with the internal climate variability, coming from the atmospheric and oceanic chaos. The concept of radiative forcing is involved in a fundamental Earth's climate equation [13-20]:

$$R(t) = F(t) - \lambda T(t) \quad (t \text{ in years}) \qquad (1)$$

In this equation, R is the radiative balance ($W\ m^{-2}$) at the top-of-atmosphere (TOA), and T is the global surface temperature deviation (*anomaly*) with respect to its expected mean value in the absence of any external or internal imbalance factor. The term $F = \sum f_i$ is the sum of the so called *radiative forcings fi* induced by imbalance factors. Coefficient λ is the *climate feedback coefficient*

and defines a fundamental metric of the Earth climate system.

Despite its apparent simplicity, this relationship is not self-evident. In a comprehensive paper on radiative forcing (more than 800 references), [20] state: *"A grand challenge in Earth system science lies in continuing to sustain the relatively simple essence of the radiative forcing concept in a form similar to that originally devised [*Eq. 1*], and at the same time improving the quantification of the forcing "*. They even evoke *"unresolved issues and grand challenge related to the viability of this concept"*.

After decades of thought and thousands of published technical studies, climate scientists are coming to challenge even the *viability* of the very concepts on which the understanding of the climate system is based. This raises the question of whether values and ranges for λ make sense. The *"chronic uncertainty in the value of λ which persist to this day"* reach indeed [0.51 to 1.81] $W\,m^{-2}\,C^{-1}$ (AR6 IPCC range).

For our part, we continue to assume that Equation 1 is constructive, and we propose to make use of the ERF (Effective Radiative Forcings) dataset involved in the CMIPs. These forcings are noted $\{u_{ant}(t),\ u_{sol}(t),\ u_{volc}(t), \cdots\}$. Even if the confidence in their quantification is weak, their temporal profile is retained, admitting that the total forcing $F = \sum f_i$ can be written through:

$$f_i \sim \alpha_i u_i \qquad (2)$$

The α_i are scaling factors to be determined, jointly with λ, in order to reach the best agreement of a *behavior model* with the *observed* climate data (not simulated from speculative models). The sequel will show that these scale factors could deviate greatly from unity, higher or lower depending on whether the data u_i over- or under-estimate the actual effective forcings.

The ERF series u_i retained for this work are shown in Figure 3. They are in conformity with the forcings shown in AR5 (2014), Chapter 8, in particular Figure 8.18.

In panel (a), anthropogenic forcing come from the Representative Concentration Pathway / Shared Socioeconomic reference Pathways (RCP / SSRP), limited to the historical period.

In panel (b), solar forcing shows oscillations with a period of about 11 years: the Schwabe solar cycles. These had been observed since 1610, but we ignore them prior to the historical period, their effects on the earlier paleoclimate period being practically insignificant.

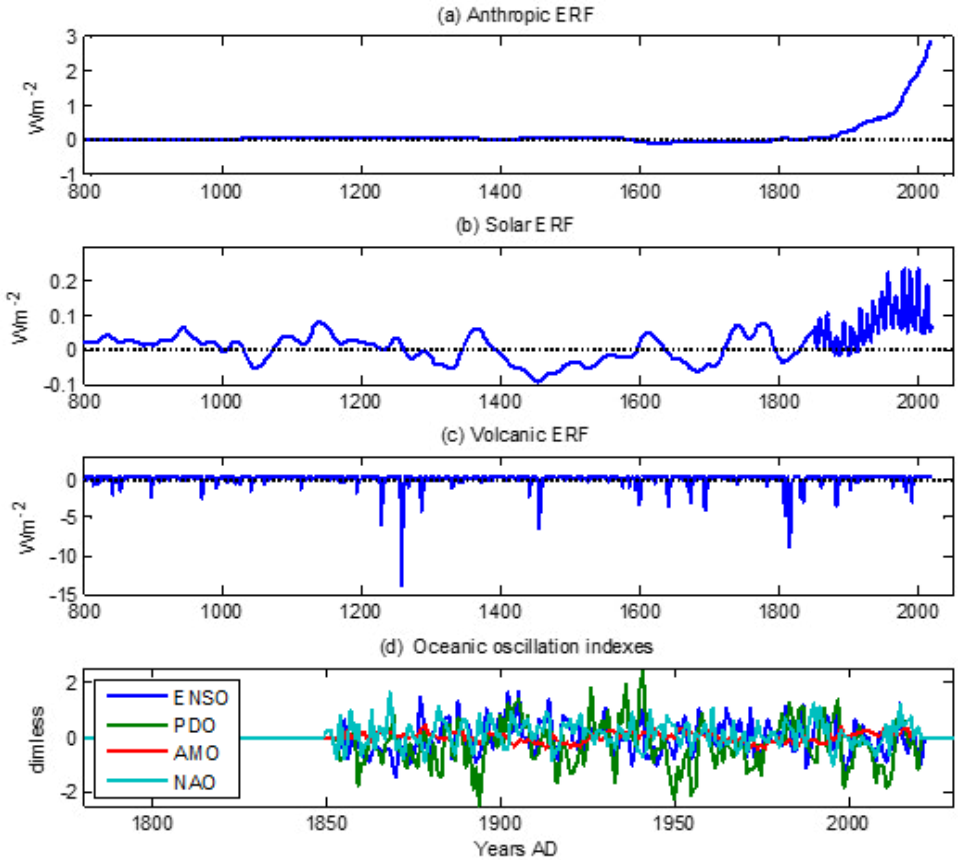

Figure 3. ERF: **(a)** Anthropogenic forcing **(b)** Solar forcing: O. Coddington, J. Lean, P. Pilewskie, (NOAA CDR Program), based on the model NRLSSI2. Before 1850 : extrapolation by alignment and calibration of the cosmogenic series 10Be [21]. **(c)** Volcanic forcing: [22]. **(d)** Internal variability indexes.

Panel (d) shows four main ocean oscillation indices: ENSO (El Niño Southern Oscillation), PDO (Pacific Decadal Oscillation), AMO (Atlantic Multidecadal Oscillation), NAO (North Atlantic Oscillation).

These indexes are based on temperature or pressure measurements at different places in the oceans. They are designed in order to be sensitive to heat distributions and surface heat fluxes generated here and there by atmospheric and oceanic chaos, while remaining insensitive to major climate variations coming from external forcings. By their very nature, their variations do not cause radiative forcings at TOA. Contrary to the external forcings, these indexes are not expressed in W^{m-2}, being dimensionless. Therefore, they cannot be combined into a global balance (as anthropogenic forcings) and must be treated separately when modeling. Similarly to the Schwabe cycles, they are taken into account only from 1850 onwards.

Behavior Climate Model (Black-Box Model)

Any reduction in model complexity must be adapted to its objectives. Per the methodology of the existing *Reduced Complexity Model Intercomparison Project* (RCMIP), the scope is limited to the simulation of global surface temperature, and the purpose from this perspective is to replicate the behavior of the complete AOGCM's: *"The validity of the RCM approach rests on the premise that RCMs are able to replicate the behavior of the Earth system and response characteristics of our most complete models"* (Nicholls et al. 2020). However, in the present study, we elected to take as reference not the simulations of the climate by complete calculation models, but directly the input-output behavior of the true climate, as revealed from historical and paleoclimate observation series.

Atmosphere-ocean Two-Layer Models (TLMs) are energy balance models (EBMs) [23, 24, 25, 26, 27]. They provide a structure that is well suited for our methodology. The causal model from the forcing inputs u_i to the output T is expressed by linear transfer functions $G_i(s)$ in the Laplace variable s (for basics in dynamic systems theory, see e.g) [28]:

$$T = \sum G_i(s) u_i \qquad (2)$$

As the state dimension of TLMs is two, the transfer functions $G_i(s)$ can be parameterized under the form:

$$G_i(s) = \frac{1}{(1+s\tau_a)} \frac{a_i + s\tau_o\ c_i}{(1+s\tau_o)} \qquad (3)$$

which is equivalent to the differential equation:

$$T + (\tau_a + \tau_o)\frac{dT}{dt} + \tau_a \tau_o \frac{d^2T}{dt^2} = \sum (a_i u_i + \tau_o c_i \frac{du_i}{dt}) \qquad (4)$$

Relationships linking the concrete parameters of a two-layer model to those of the above model are detailed in the appendix. Regardless of these relationships, the parameters τ_o, τ_a, a_i, c_i drive the responses to a unit step input ui, as shown in Figure 4, where $a_i = 0.9°C\,m^{-2}$, $c_i = 0.6°C\,m^{-2}$, $\tau_a = 1\,yr$, $\tau_o = 100\,yr$.

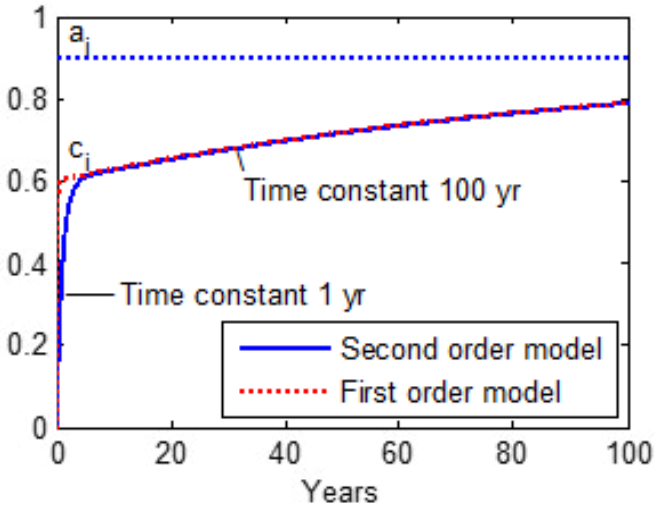

Figure 4: *Unit step responses. First order: limit for* $\tau_a = 0$

Time Constants

The time constants τ_o and τ_a are not *i*-indexed, being the same for all transfer functions. They aggregate the respectively slow and fast dynamics governing oceans and atmosphere behavior. For atmosphere, τ_a ranges from a few months to a few years. In the oceans, τ_o covers hundreds of years. These are not uncertainty ranges, but continuums of coexisting time constants. We fix *a priori* τ_o and τ_a according to the temporal domain to be favored by the model. For example, if we want to obtain the better behavior in response to quasi-impulse inputs (e.g. volcanic activity signals), we will set $\tau_a = 1\ yr$ (or even $\tau_a = 0$). Simultaneously, to favor very long-term climate modeling, one selects τ_o in the high range of the

assumed ocean continuum, e.g., $\tau_o = 300\ yrs$ (or more). For the secular horizon behaviors (those of interest to policy makers) we prefer $\tau_o = 100\ yrs$.

In the end, the values we obtain for λ and the $\alpha_i s$ will depend on the arbitrary values given to τ_o and τ_a.

Equilibrium and Short-Term Sensitivities

Parameters $a_i = G_i(0)$ are static gains, namely the equilibrium sensitivities to the radiative forcings u_i. In the ideal case where the given radiative forcings are exactly calibrated $(u_i = f_i)$, the a_i would all be equal to $1/\lambda$, the inverse of the climate feedback coefficient. Otherwise, they are a priori different: $a_i = \alpha_i / \lambda$.

The ratio of short-term sensitivity to equilibrium sensitivity is given by, c_i / a_i as shown in Figure 4 where $c_i / a_i = 2/3$, which is roughly consistent with the simulated responses to abrupt CO_2 changes in the CMIP projects.

Reducing the imbalance factors to their radiative forcing alone suggests that the c_i / a_i ratios should be the same. In fact, the physical mechanisms are not the same for all the forcings. For example, a change in GHG concentration first affects the atmosphere, resulting in a high short-term sensitivity (e.g. $c_{anth} / a_{anth} \sim 2/3$), while a change in solar irradiance first causes warming of the oceans, hence $c_{sol} / a_{sol} << 1$.

External Forcings Versus Internal Variability

The fundamental difference between external radiative forcings and internal variability indexes is that the latter do not impact climate equilibrium. They are therefore subject to the constraint $a_i = 0$. The oceanic indexes u_i being dimensionless, the corresponding parameters c_i are expressed in $°C$.

Identification

Parameters estimation of a black-box model from the series of input and output data fall under the theory of *dynamic systems identification* [29, 30, 31, 32, 33, 34, 35, 36]. The variety of methods allows to reach statistical optimality (the so called ARMAX, B&J, PEM methods, etc.) or to simplify the implementation (as ARX, OLS).

In the present case, given τ_a, τ_o and the input series $\{u_i\}$, the parameters $\{a_1, a_2, \cdots c_1, c_2, \cdots\}$ linearly impact the output T of the model. Then, the identification by the method known as the Output Error (OE) reduces to a linear regression.

Scaling Factors and Climate Feedback

The input output data $\{u_i\}$ and T alone do not allow obtaining the climate reaction coefficient λ nor the scaling factors α_i associated with the real forcings. To evaluate them, we use an additional set of observations consisting in the oceanic heat content $Q(t)$, known in particular from the Argo system. Assuming negligible the heat capacities of the atmosphere, the continental surface and the cryosphere, $Q(t)$ represents practically the total heat content of the climate system, then:

$$dQ / dt = R \tag{5}$$

We substitute the relation $\alpha_i = \lambda\ a_i$ in the expression $R = \sum \alpha_i u_i - \lambda T$. The a_i and b_i, having been determined previously, we built the signal $U(t) = \int_{t_0}^{t} \left[\sum a_i u_i(\tau) - T(\tau)\right] d\tau$ by numerical integration of the given series $u_i(t)$ and $T(t)$. Hence the following equation:

$$Q(t) = Q(t_0) + \lambda U(t) \tag{6}$$

Then Q(to) and λ are estimated by linear regression, which gives $\alpha_i = \lambda a_i$

Preindustrial Temperatures

By convention, the zero level of the radiative forcing series are defined here as their pre-industrial mean (850-1850). Figure 3 follows this convention. On the other hand, the given temperatures (Figure 2) are some anomalies with respect to arbitrary reference periods. Their zeros do not correspond to the pre-industrial equilibrium temperatures (assumed to be at zero radiative forcing). When identifying, each temperature series is then accompanied by an unknown defined as the associated pre-industrial temperature, *a priori* different for the historical and paleoclimatic series. These unknowns are identified in the same way as the model parameters.

When comparing with the simulated outputs, the given temperatures are then corrected by their respective estimated pre-industrial temperatures. This operation thus realizes the alignment between the paleoclimate reconstructions and the historical temperatures, operation made difficult by the so-called divergence problems [37, 38].

Ranges and Probabilities

The uncertainty ranges given thereafter are, as in the IPCC reports, 90% confidence intervals (+/– 1.64 σ). Our calculation [36] involves the full autocorrelation function of the output error. Although they do not cover all causes of uncertainty, these confidence intervals nevertheless provide an objective indication, free of subjective bias.

Validation of the Behavioral Model

This section resumes the conditions of Figure 1-a : low PCA paleoclimate reconstruction, scaling factors constrained to αi = 1, which implies $a_{anth}, = a_{sol} = a_{volc} = 1/\lambda$ The internal variability indexes being not yet included here, the only degrees of freedom are now the coefficients $\{a_{anth}, c_{anth}, c_{sol}, c_{volc}\}$ and the pre-industrial equilibrium temperatures (historic and paleoclimatic).

Coefficient c_{anth} is left free. Then, constraint $c_{sol} > 0$ is set since an increase in solar forcing necessarily increase temperature. On the other hand, volcanism leads to some inconsistent data. For example the huge Samalas eruption (1257) has a little impact compared

the historical flares. The value $c_{volc} = 0.10$ is arbitrarily set to obtain admissible responses response to recent flares, the long term responses remaining driven by a_{volc}.

To perform identification, we constrain $a_{anth}, = a_{sol} = a_{volc} = 1/\lambda_0$ where λ_0 is adjusted until $\alpha_i = 1$ is return by identification. This leads to:

$$a_{anth} = a_{sol} = a_{volc} = 0.495 \ \ ^\circ C\, W\, m^{-2}$$

$$c_{ant} = 0.36 \ ^\circ C\, W\, m^{-2},\ c_{sol} = 0,\ c_{volc} = 0.1$$

The ratio $c_{anth} / a_{anth} \sim 0.7$ is consistent with the CMIP simulations. The constraint $c_{sol} > 0$ is reached, which will be explained. The identified climate response coefficient λ slightly overcomes the AR6 upper limit (TS 2021, p. 95):

Estimated : $\lambda = 2.04$ [1.98 2.10] $Wm^{-2}\ ^\circ C^{-1}$
AR6 : $\lambda = 1.16$ [0.51 1.81] $Wm^{-2}\ ^\circ C^{-1}$

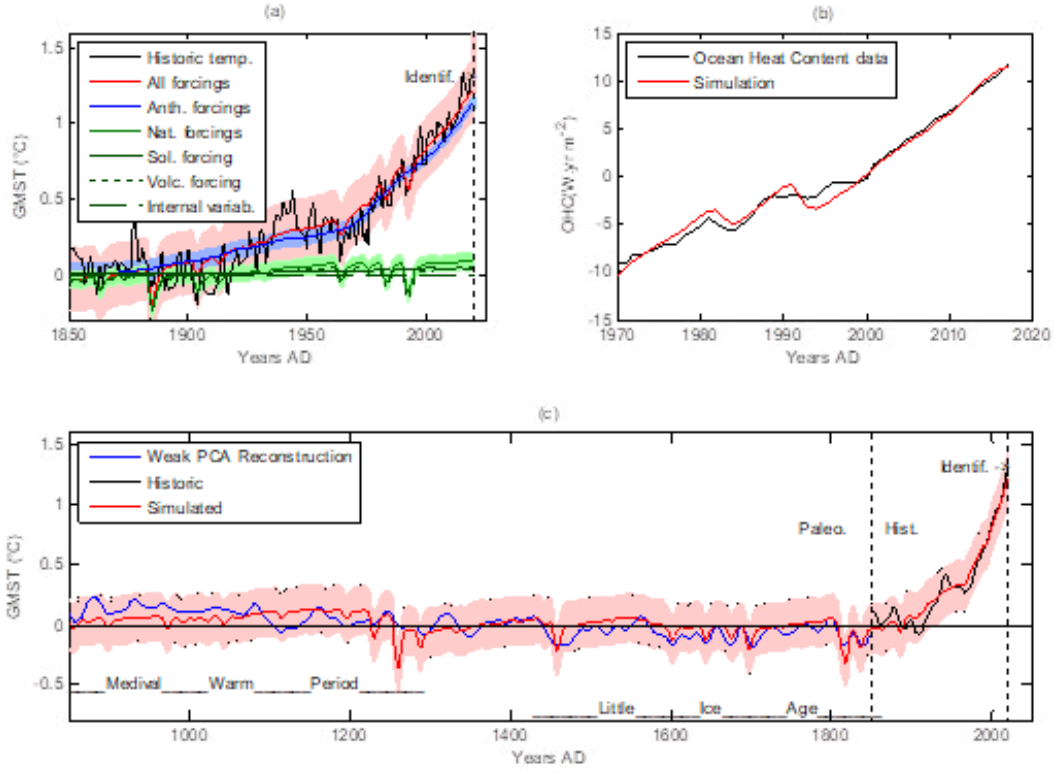

Figure 5. *Identification from low PCA paleoclimate temperature. (a) : historic period temperatures. (b) : ocean heat content. (c) : whole period.*

Simulation results are shown in Figure 5. The panel (a) is the same as Figure 1-a, except for the addition of the uncertainty ranges for the simulated temperature (red) as well as for the anthropogenic (blue) and natural (green) contributions. The thin lines detail the natural contributions: solar, volcanic and internal variability, the latter being assumed to be null Panel (b) shows the reconstruction of the ocean heat content (data from) [39]. Note the replication of the impacts of the volcanic eruptions of 1882 and 1991 (El Chinchon and Pinatubo).

Panel (c) shows the simulation of paleoclimate temperatures. They are smoothed for readability and are very similar to the AR6 simulations (Technical summary, Box TS.2. Figure 2-b). Volcanic activity contributes to the reproduction of the Little Ice Age (1500-1850).

The similarity of our figure 5-a with Figure 1-b of the Summary for Policymakers (SPM) of AR6 (Assessment Report 6) of IPCC (2021) is striking. This ability to replicate the global behavior of complex climate models confirm the soundness of our model of weak complexity, not only according to the RCMIP criteria, but more importantly by its ability to replicate the climate observations.

However, there is something troubling. Taking the usual value 3.7 $W\, m^{-2}$ for the radiative forcing at CO_2 doubling, then the formula ECS $= 3.7/\lambda$ gives the equilibrium climate sensitivity:

$$ECS = 1.81\ [\ 1.76 \text{ to } 1.87]\ ^\circ C$$

This range is low, but within that of AR5 (1.5 $^\circ C$ to 4.5 $^\circ C$). Conversely, it is outside that of the AR6 (2.5 $^\circ C$ to 4$^\circ C$).The lower

bound strongly increased between 2013 and 2021. However there have been no major revisions in the data sets (forcings, global temperature, ocean heat content) that would explain such a shift in the IPCC lower limits.

Inconsistency Between Anthropogenic Principle and PCA

An important question now arises: is it possible to reproduce paleoclimate reconstructions at high PCA while respecting the anthropogenic principle? None of our attempts succeeded, when keeping the constraints $\alpha_i = 1$ on forcing factors: the pre-industrial simulation remains that of a low PCA. To our knowledge, CMIPs do not succeed either. This two failures suggest an intrinsic incompatibility between the anthropogenic principle and the existence of non-negligible pre-industrial temperature variations.

In this section, we optimize the model on the basis of a strong PCA. The coefficients a_i and c_i, including the oceanic oscillation indexes are now left free, except the following constraints. The first is the ratio $c_{anth}/a_{anth} = 0.66$, according to the CMIP simulations, the others are, as in Section 6, $c_{sol} > 0$ and $c_{volc} = 0.1$.

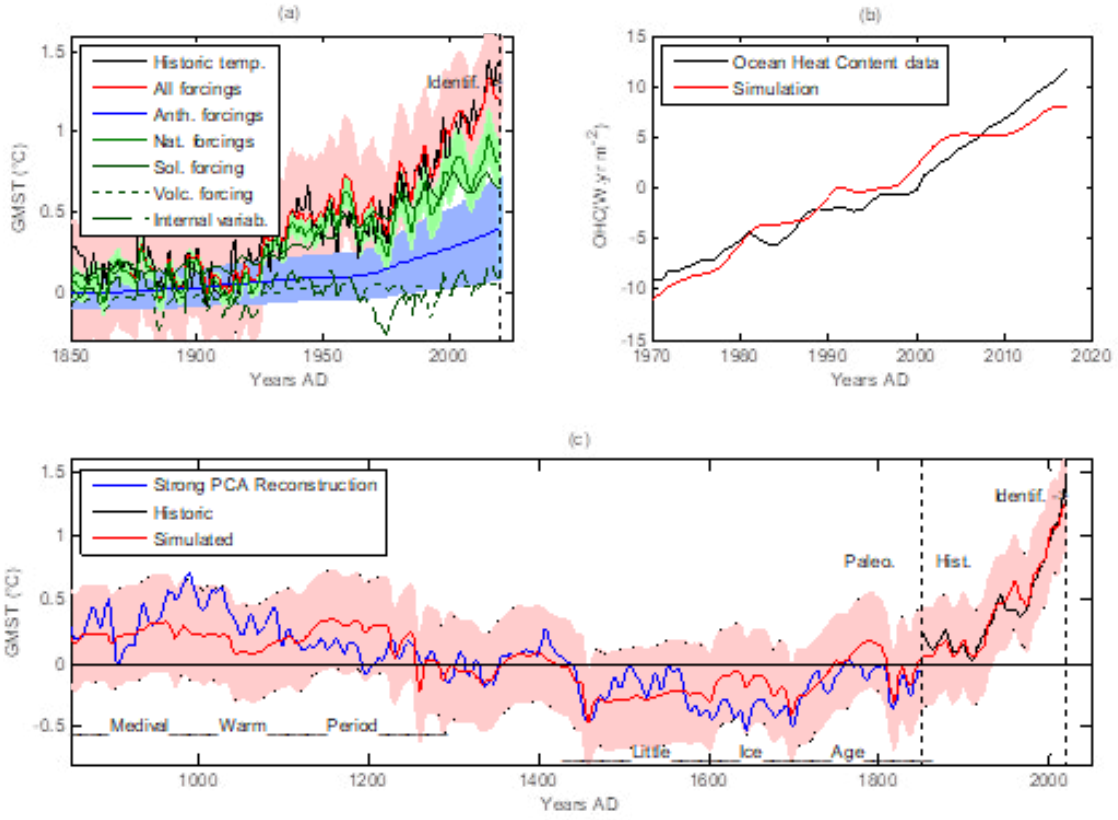

Figure 6: *Strong PCA Simulations*

First, note two minor shortcomings in the simulations of Figure 6. In panel (a) the solar contribution (line —), shows contributions from Schwabe cycles that have no apparent relation with observations. Similarly, in panel (c), the peaks at years 1970, 1982, 1995, 2005 show a contribution of the same cycles, non-existing on observations. These defects will be dealt with in Section 8.

Note also that the internal variability (line – –) contributes to the climate variations: mid century cooling and last warming, thus weakening the anthropogenic principle. Own to the incorporation of the ENSO index, we also obtain a better follow-up of interannual variations.

Panel (c) illustrates the reproduction of the pre-industrial climate anomalies (MWP and LIA). The residual deviations may result from both uncertainties in the temperature proxies and internal variability. They are of a higher level than those in Figure 5. It follows the larger uncertainty ranges shown in Figure 6.

The key point is that, despite these enlarged uncertainty ranges, the simulations in panel (a) are in irreducible contradiction with the anthropogenic principle, since the anthropogenic contribution to warming is now substantially lower than the natural contributions. This result cannot be rejected on principle: it comes from observations, not from speculative physical models. They are consistent with the following estimated scaling factors:

$\alpha_{anth} = 0.127$ [0.06 to 0.20]
$\alpha_{sol} = 5.32$ [3.18 to 7.46]
$\alpha_{volc} = 0.406$ [-0.034 to 0.85]

λ = 0.632 [0.559 to 0.705] $Wm^{-2}\,°C^{-1}$

The climate feedback λ is now within the IPCC range (0.51 to 1.81). Applying the corrected formula $ESC = \alpha_{anth}\ 3.7 / \lambda$ leads to the *ESC* range:

$$ESC = 0.74\ \ [0.31 \text{ to } 1.32]\ °C$$

which is very low compared with the last IPCC assessments (2.5 °C to 4.5 °C).

The key problem is thus the plausibility of an overestimation of the given anthropogenic forcing u_{anth} in a ratio up to eight ($u_{anth} / f_{anth} = 1 / \alpha_{anth} \sim 8$).

In Section 3 we have already question the very concept of forcing. To go further, consider the likely range indicated in AR6 for the total anthropogenic forcing increase between 1750 and 2019 (SMP p. 11, A.4.1). It ranges from 1.96 to 3.48 Wm^{-2}. The ratio between the lower and upper bounds is close to 2. It is substantial, but still far from an eight-to-one ratio.

One of the main components of anthropogenic forcing results from greenhouse gases, especially CO_2. The radiative transfer codes (HITRAN, MODTRAN) allow the theoretical calculation of the radiative forcing at TOA (primitively at the troposphere) from the standard US atmosphere profile, or other ones depending on latitude, cloud cover, etc. The general formula is $f_{co2} = \rho \log_2(ppm / ppm_0)$ where ρ is the change in forcing resulting from a doubling the CO_2 concentration (*ppm*: parts per million). For the standard US profile, ρ would be about 3.7 $W\,m^{-2}$.

This forcing is defined as an *Instantaneous Radiative Forcing* (IRF), while the given forcing series refer to *Effective Radiative Forcings* (ERF). These embed the short time feedbacks leading to the effective atmospheric equilibrium induced by IRF, the mean surface temperature being assumed to be constant. Figure 14.5 in [20] shows some steps between IRF to ERF, but the list of all adjustments is far from complete. For example, GHG-induced RFI is localized in the upper atmosphere. This can dissipate high altitude clouds, and thus decrease the absorbed solar flux, implying a negative effect on the ERF, involving itself new feedbacks. The assessment is impossible otherwise than by simulations based on complete general circulation models, the same ones that are being validated. Despite the large uncertainties inherent in these calculations, the universally accepted value since remains 3.7 ± 0.5 $W\,m^{-2}$ at doubling CO2, without the formula ever having been substantially revised since, neither in its form (log) nor in its quantification (3.7 ± 0.5 $W\,m^{-2}$ in IPCC AR6, TS p92) [40].

Moreover, *fco2* is only one of the components of the whole anthropogenic forcing f_{anth}. Other factors add their own uncertainties and some of which (aerosols, land use change) have antagonistic effects to GHGs. In the event where the resulting lower range could approach zero, there is no longer an upper limit to the ratio $1/\alpha_{anth}$.

Finally, questioning the plausibility of the obtained scale factor α_{anth} also raises the issue of the given CMIP ranges and their degree of objectivity. Recall that for IPCC, *"the probability of an event is the degree of belief that exists among [ours] lead authors and reviewers that the event will occur [...] When complex systems are the topic, both prior and updated probability distributions usually contain a high degree of (informed) subjectivity"* [41]. In any case, it must be claimed that updated probabilities (based on observations) must prevail over any subjective prior distribution. In view of all these considerations, a strong overestimation of anthropogenic forcing cannot be ruled out.

Is Solar Activity the Main Driver of Climate Change?

Let us now consider the identified scaling factor α_{sol} = 5.28. It reflects a possibly strong underestimation of the given solar activity. Table 7.8 of AR6 states that the present solar ERF relative to the reference date 1750 would be 0.01 [– 0.06 to 0.08] $W\,m^{-2}$. Not only possibly negative, it appears as completely negligible compared to the anthropogenic forcing over the same period: 2.72 [1.96 to 3.48] $W\,m^{-2}$. Interestingly, the beginning of the above reference period (1750) just lies within a local maximum between the Maunder (1700) and Dalton (1820) solar minima (see Fig. 7). It follows that the indicated range is formally exact, but illusive. It tends to minimize variations of solar ERF, thereby increasing the relative contribution of the anthropogenic factors.

Also, the solar activity does not necessarily play only through the Total Solar Irradiancy (TSI), but also its spectral distribution. Let us mention also the variations of the solar magnetism [42], its shield effects towards cosmic radiation, impacting the genesis of clouds [43,44], the solar wind generated by solar flares for comprehensive reviews [45, 46]. Although these processes are not yet sufficiently well modeled to be incorporated into the physical models of CMIPs, it does not follow that they are inexistent. The scaling factor α_{sol} could take them into account. However, multiplying the whole signal u_{sol} it results in a strong amplification of the Schwabe variations, hence the untimely effects shown in Figure 6-b. A solution was to introduce two different scaling factors depending on the high or low frequency of the solar forcing [38].

Another question relates to the TSI reconstructions themselves. They combine modern satellite measurements (since 1978), sunspot observations (since 1610) and millennial cosmogenic proxies (14C, 10Be). The quantifications of the high-frequency components of the TSI match well each other over the recent period. Conversely, the low frequency variations are highly uncertain, even for the decades from 1978. Indeed, there is no direct measurement of TSI before 1978, let alone in paleoclimate times, not even an order of magnitude. Various empirical solar models (listed in Figure 7) calibrate the solar proxies (sunspots, cosmogenics) on modern measurements, themselves uncertain. This results in the sparse reconstructions of Figure 7 (data provided by T. Egorova), centered here on their 2000-2020 mean. The NRL reconstruction is precisely that leads to Figure 3-b, used in previous sections.

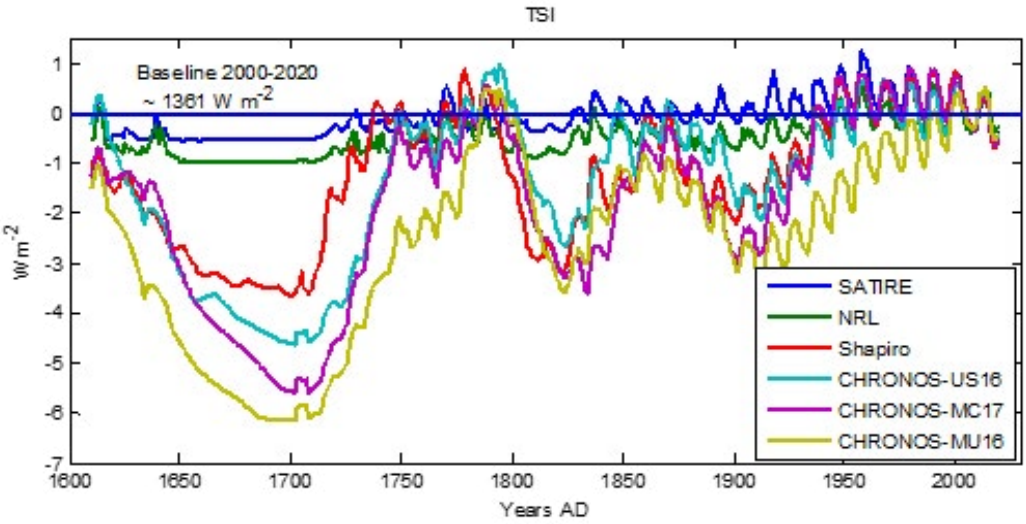

Figure 7. *TSI Reconstructions per increasing low frequencies magnitudes.*

Models: SATIRE (Spectral and Total Irradiance Reconstruction, Yeo et al. 2014); NRLTSI2 (Naval Research Laboratory Spectral Solar Irradiance, Coddington et al. 2016); Shapiro (2011); CHRONOS-XX (Code for the High spectral Resolution reconstruction of Solar irradiance, [47].

The Shapiro series was challenged in AR5 (8SM11): *" indicates that temperature simulations driven by such a large solar forcing are inconsistent with reconstructed and observed historical temperatures" [48].* In fact, per the above analysis, the inconsistency results from an excessive total in radiative forcings at the input of the models, with no evidence to attribute this excess to the sun rather than to human action. AR6 (Chap. 2.2) estimates typical millennial-scale TSI magnitudes at 1.5 [1.4 to 2.1] $W\,m^{-2}$, which leads to restrict the reconstructions to the only SATIRE and NRL2, the most consistent with to the anthropogenic principle. Moreover, according to AR6, *"Although stronger variations in the deeper past cannot be ruled out completely there is no indication of such changes having occurred over the last 9 kyr" [47,49].* But precisely, the temperature observations of our common era constitute such an indication, in as much as temperature reconstructions with a non-negligible PCA are envisioned.

This led us to resume the model identification with the CHRONOS-MU16 reconstruction – the one that maximally amplifies the low frequency components of the TSI. We obtain the following scaling factors:

α_{anth} = 0.219 [0.165 to 0.27]
α_{sol} = 1.19 [0.809 to 1.58]
α_{volc} = 0.462 [0.005 to 0.92]

The value $\alpha_{anth} << 1$ confirms that the anthropogenic forcing reconstruction remains strongly overestimated by CMIP. In contrast, the solar scaling factor α_{sol} is now close to 1, confirming the likelihood of the CHRONOS reconstructions. The simulations (not shown here) remain close to those of Fig. 6. Due to the strong increase in solar secular frequencies, the PCA is well reproduced, while the decadal frequencies are not amplified (see Fig. 7), so that the climate responses are now free of the Schwabe contributions reported Fig. 6-a and -b.

The estimated climate feedback coefficient remains of the same order: = 0.709 [0.684 to 0.734] $Wm^{-2}°C^{-1}$. Then the climate sensitivity slightly increases compared to that of section 7:

$$ECS = 1.14\ [0.83\ \text{to}\ 1.36]\ °C$$

Nevertheless, it remains completely outside of the AR6 assessed likely range of 2.5°C to 4°C.

Conclusion

In section 8 above, a set of consistent climate series is explored, from which solar activity appears to be the main driver of climate change. To eradicate this hypothesis, the anthropogenic principle requires four simultaneous assessments:

- A strong anthropogenic forcing, able to account for all of the current warming.
- A low solar forcing.
- A low internal variability.
- The nonexistence of significant pre-industrial climate anomalies, which could indeed be explained by strong solar forcing or high internal variability.

None of these conditions is strongly established, neither by theoretical knowledge nor by historical and paleoclimatic observations. On the contrary, our analysis challenges them through a weak complexity model, fed by accepted forcing profiles, which are recalibrated owning to climate observations. The simulations show that solar activity contributes to current climate warming in proportions depending on by the assessed pre-industrial climate anomalies. Therefore, adherence to the anthropogenic principle requires that when reconstructing climate data, the Medieval Warming Period and the Little Ice Age be reduced to nothing, and

that any series of strongly varying solar forcing be discarded.

Appendix. Equivalence black-box – two-layer models

The formulation of the black box model through a second order transfer function is justified first by its operational efficiency. Its equivalence with a two-layer model allows concretizing the underlying climate mechanisms and parameters.

Equations

The state vector of a two-layer model (TLM) is reduced to the atmospheric and oceanic heat contents Q_a and Q_o ($W\,yr\,m^{-2}$). Let R be the radiative imbalance at TOA and S the energy balance across the surface. The law of conservation of energy is written:

$$\frac{dQ_a}{dt} = R - S \qquad \frac{dQ_o}{dt} = S$$

For *R*, we return to the basic expression:

$$R = -\lambda T + F$$

where λ is the climate feedback coefficient and $F = \Sigma \alpha_i u_i$ is the total TOA radiative forcing. Similarly, S is written:

$$S = \mu T - \nu T_o + G$$

where *m* and ν are heat exchange coefficients, T_o an oceanic temperature to be defined, and *G* a *forcing at the BOA* (Bottom Of Atmosphere), or *surface forcing* (AR4 2.2,) [50, 51]. Surface forcings are commonly ignored in two-layer models. Actually, GHGs cause no or little surface forcings, but in general these forcings do exist (especially for solar activity), and they explain the differences in the transient responses to different forcing factors. It is emphasized that surface forcings are not strictly radiative. For example, land use change impacts *S* through albedo and evapotranspiration. In the same way we developed $F = \Sigma \alpha_i u_i$, we write:

$$G = \Sigma \beta_i u_i$$

Assume now that there exists mean temperatures Ta, To and thermal inertias Ca, Co such that:

$$Q_a = C_a T_a \quad Q_o = C_o T_o$$

Most of the atmospheric heat is located in the troposphere, where the lapse rate is roughly constant (–6.5 °*C/km*). We can therefore consider that the global surface temperature *T* equals T_a (to within a constant). Conversely, T_o is not observed, but only the product $Q_o = C_o T_o$. Then redefine $T_o := (\mu/\nu)T_o$, $C_o := (\nu/\mu)C_o$ which leaves unchanged Q_o and leads to $\nu = \mu$.

Then, with (T, T_o) as state vector, the TLM state space equations becomes

$$\begin{bmatrix} dT_a/dt \\ dT_o/dt \end{bmatrix} = \begin{bmatrix} -(\lambda+\mu)/C_a & \mu/C_a \\ \mu/C_o & -\mu/C_o \end{bmatrix} \begin{bmatrix} T_a \\ T_o \end{bmatrix} + \begin{bmatrix} (1/C_a)\Sigma(\alpha_i - \beta_i) \\ (1/C_o)\Sigma\beta_i \end{bmatrix} u_i$$

$$\begin{bmatrix} T \\ Q_o \end{bmatrix} = \begin{bmatrix} 1 & 0 \\ 0 & C_o \end{bmatrix} \begin{bmatrix} T_a \\ T_o \end{bmatrix} \quad (\textit{to within constants})$$

Figure 8 convert the above equations into a causal bloc diagram, directly transposable into a simulation scheme (e.g.Matlab-Simulink®).

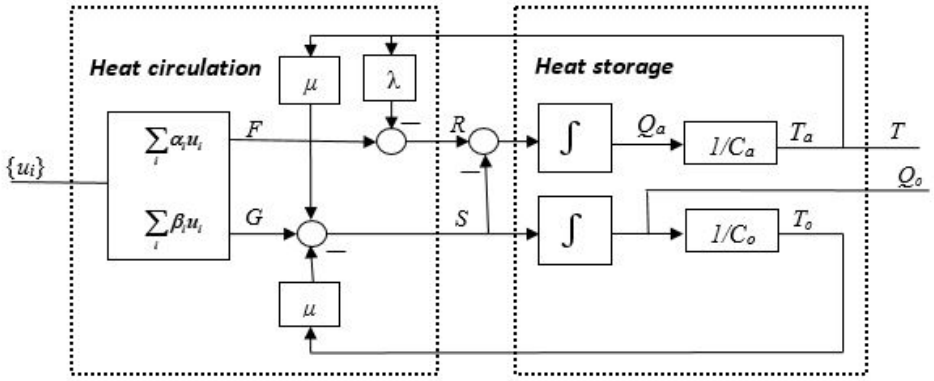

Figure 8: Block diagram of a two-layer model

Interpretation

Coefficients C_a, C_o, α_i, β_i, with λ and μ, are the *'physical'* parameters associated with the two-layer model. This raises the question of the concrete sense of the parameters α_i, β_i. These have meaning only in their relation to the signals u_i. While *T* and Q_o are direct observations, the u_i signals are constructed from measurements, some of them objective (GHG concentrations, TSI) and others more or less indirect (change of land use, various proxies).

The interpretation of α_i as scaling factors presupposes some validity of these u_i as ERFs, but in the behavioral approach, they reduce as to indicators of the various imbalance factors, whose only the profiles are retained, without consideration of their nature and units.

These factors have direct impacts, not only on the fluxes at the TOA, but also at the BOA. The β_i provide the two-layer models with the required degrees of freedom, without which they are incapable of correctly representing the observed climate behaviors.

Furthermore, the input-output behavior reduced to the couple (u_i, *T*) does not allow identifying individually all the physical parameters, but only the behavioral ones. This is why we had to

use the second output Q_o shown in figure 8.

These contributions to the reduction of complexity of climate models are an essential contribution of this paper, without which the evaluation of AGW cannot be completed. The major contribution is eq. $G = \Sigma \beta_i u_i$, which was not yet introduced in de [52,38].

Conversion Black Box - TLM

The transfer function of the physical model (input u_i, output T) is straightforward through formal conversion of state space form into transfer form:

$$G_i(s) = \frac{s(\alpha_i - \beta_i)/C_a + \alpha_i \mu/(C_a C_o)}{s^2 + s(\lambda+\mu)/C_a + \mu/C_o) + \lambda\mu/(C_a C_o)}$$

It identifies with the behavioral model:

$$G_i(s) = \frac{1}{(1+s\tau_a)} \frac{a_i + s\tau_o \; c_i}{(1+s\tau_o)}$$

The direct conversion of the TLM parameters C_a, C_o ,α_i, β_i , λ and μ, into the behavior coefficients τ_a, τ_o, a_i, c_i is given by:

$$[\tau_a^{-1}, \tau_a^{-1}] = -\text{roots}(s^2 + s(\lambda+\mu)/C_a + \mu/C_o) + \lambda\mu/(C_a C_o))$$

$$a_i = \alpha_i/\lambda \quad c_i = (\alpha_i - \beta_i)C_o/\tau_o/\lambda/\mu$$

Conversely, to trace the six physical parameters C_a, C_o ,α_i, β_i, λ , μ from the five fixed or identified coefficients τ_a, τ_o, a_i, c_i, λ , an additional information is required. If μ is given, the exact inverse formulas are:

$$C_o = \max(roots\left[x^2 - (\tau_o + \tau_a)\frac{\mu\lambda}{\mu+\lambda}x + \tau_o\tau_a\frac{\mu^2\lambda}{\mu+\lambda}\right]) \quad C_a = \tau_a\tau_o\mu\lambda/C_o$$

$$\alpha_i = \lambda\, a_i \quad \beta_i = \alpha_i - c_i\tau_o\mu\,\lambda/C_o$$

These tedious expressions are confirmed through direct and inverse numerical conversions.

Getting μ

Consider a radiative forcing u_0 among those for which the surface forcing is assumed to be zero, typically the GHG concentrations. Let (a_0, c_0) be the corresponding pair. By setting $\beta_0 = 0$, and identifying the two formulations of $G_i(s)$, we obtain μ from the following exact expression:

$$\mu = \lambda\left(\frac{a_0 - c_0}{c_0}\right)\left(\frac{c_0 - \tau_a\tau_o^{-1}a_0}{c_0}\right)$$

Numerical Approximations

In default of obtaining (a_0, c_0) by identification, a great amount of simulations from CMIPs are available. Despite some dispersion, the responses to abrupt change in CO2 are similar to Figure 4 and the ratios c_0/a_0 are near 2/3 (see) [26,53].

For $\tau_a << \tau_o$ the above expression becomes: $\mu \sim \lambda\frac{a_0 - c_0}{c_0}$. Then the atmosphere-ocean exchange coefficient is approximately half the climate feedback coefficient: $\mu \sim \lambda/2$.

Moreover, for $\tau_a << \tau_o$, C_a and C_o becomes :

$$C_a \sim \tau_a(\lambda+\mu), \; C_o \sim \tau_o\frac{\lambda\mu}{\lambda+\mu}$$

Then, for $\mu \sim \lambda/2$:

$$C_o \sim \tau_o\lambda/3 \;\; C_a \sim 3\,\tau_a\mu \;\; \beta_i \sim \lambda(a_i - 1.5\; c_i)$$

Given the orders of magnitude $\tau_o = 100\,yr$ and $\lambda \sim 1\; W\,m^{-2}\,°C^{-1}$, we obtain $C_o \sim 33\; Wyr\,m^{-2}\,°C^{-1}$. Actually, the thermal inertia calculated from the whole mass of oceans is much higher: $350\; Wyr\,m^{-2}\,°C^{-1}$. This is due to the thermal stratification which inhibits temperature variations in the deep ocean. Concretely, the above C_o inertia corresponds to the 360 first meters of the oceans [54-72].

Declarations

Funding

The author declares that no funds, grants, or other support were received during the preparation of this manuscript.

Competing Interests

The authors have no relevant financial or non-financial interests to disclose.

References

1. Masson-Delmotte, V., Zhai, P., Pirani, A., Connors, S. L., Péan, C., Berger, S., ... & Zhou, B. (2021). Climate change 2021: the physical science basis. Contribution of working group I to the sixth assessment report of the intergovernmental panel on climate change, 2.
2. Le Roy Ladurie, E. (1967). Histoire du climat depuis l'an mil. Nouvelle Bibliothèque Scientifique (France) fre.
3. Soon, W., & Baliunas, S. (2003). Proxy climatic and environmental changes of the past 1000 years. Climate Research, 23(2), 89-110.
4. Lamb, H. H. (2002). Climate, history and the modern world. Routledge.
5. Mann et. al.(1998) proxy data base and northern hemispheric average temperature series. Energy & environment, 14(6), 751-771.
6. McIntyre, S., & McKitrick, R. (2003). Corrections to the Mann et. al.(1998) proxy data base and northern hemispheric average temperature series. Energy & environment, 14(6), 751-771.
7. Masson-Delmotte, V., Schulz, M., Abe-Ouchi, A., Beer, J., Ganopolski, A., Gonzáles Rouco, J. F., ... & Timmermann, A. (2013). Information from paleoclimate archives.
8. Neukom, R., Barboza, L. A., Erb, M. P., Shi, F., Emile-Geay, J., Evans, M. N., ... & PAGES 2k Consortium. (2019). Consistent multidecadal variability in global temperature reconstructions and simulations over the Common Era, Nat. Geosci., 12, 643–649.
9. Moberg, A., Sonechkin, D. M., Holmgren, K., Datsenko, N. M., & Karlen, W. (2005). 2,000-year Northern Hemisphere

temperature reconstruction. IGBP PAGES/World Data Center for Paleoclimatology Data Contribution Series, 19.
10. Loehle, C., & McCulloch, J. H. (2008). Correction to: A 2000-year global temperature reconstruction based on non-tree ring proxies. Energy & Environment, 19(1), 93-100.
11. Ljungqvist, F. C. (2010). A new reconstruction of temperature variability in the extra-tropical Northern Hemisphere during the last two millennia. Geografiska Annaler: Series A, Physical Geography, 92(3), 339-351.
12. Christiansen, B., & Ljungqvist, F. C. (2012). The extra-tropical Northern Hemisphere temperature in the last two millennia: reconstructions of low-frequency variability. Climate of the Past, 8(2), 765-786.
13. Schneider, S. H., & Dickinson, R. E. (1974). Climate modeling. Reviews of Geophysics, 12(3), 447-493.
14. Hansen, J., Lacis, A., Rind, D., Russell, G., Stone, P., Fung, I., ... & Lerner, J. (1984). Climate sensitivity: Analysis of feedback mechanisms. Climate processes and climate sensitivity, 29, 130-163.
15. Cess, R. D., Potter, G. L., Blanchet, J. P., Boer, G. J., Del Genio, A. D., Deque, M., ... & Zhang, M. H. (1990). Intercomparison and interpretation of climate feedback processes in 19 atmospheric general circulation models. Journal of Geophysical Research: Atmospheres, 95(D10), 16601-16615.
16. Gregory, J., Ingram, W. J., Palmer, M. A., Jones, G. S., Stott, P. A., Thorpe, R. B., ... & Williams, K. D. (2004). A new method for diagnosing radiative forcing and climate sensitivity. Geophysical research letters, 31(3).
17. Forster, P., Ramaswamy, V., Artaxo, P., Berntsen, T., Betts, R., Fahey, D. W., ... & Whorf, T. (2007). Changes in atmospheric constituents and in radiative forcing. Climate Change 2007: The Physical Science Basis. Contribution of Working Group I to the 4th Assessment Report of the Intergovernmental Panel on Climate Change.
18. Andrews, T., Gregory, J. M., Webb, M. J., & Taylor, K. E. (2012). Forcing, feedbacks and climate sensitivity in CMIP5 coupled atmosphere-ocean climate models. Geophysical research letters, 39(9).
19. Sherwood, S. C., Bony, S., Boucher, O., Bretherton, C., Forster, P. M., Gregory, J. M., & Stevens, B. (2015). Adjustments in the forcing-feedback framework for understanding climate change. Bulletin of the American Meteorological Society, 96(2), 217-228.
20. Ramaswamy, V., Collins, W., Haywood, J., Lean, J., Mahowald, N., Myhre, G., ... & Storelvmo, T. (2019). Radiative forcing of climate: the historical evolution of the radiative forcing concept, the forcing agents and their quantification, and applications. Meteorological Monographs, 59, 14-1.
21. Delaygue, G., & Bard, E. (2011). An Antarctic view of Beryllium-10 and solar activity for the past millennium. Climate Dynamics, 36, 2201-2218.
22. Crowley, T. J., & Unterman, M. B. (2013). Technical details concerning development of a 1200 yr proxy index for global volcanism. Earth System Science Data, 5(1), 187-197.
23. Williams, K. D., Ingram, W. J., & Gregory, J. M. (2008). Time variation of effective climate sensitivity in GCMs. Journal of Climate, 21(19), 5076-5090.
24. Held, I. M., Winton, M., Takahashi, K., Delworth, T., Zeng, F., & Vallis, G. K. (2010). Probing the fast and slow components of global warming by returning abruptly to preindustrial forcing. Journal of Climate, 23(9), 2418-2427.
25. Winton, M., Takahashi, K., & Held, I. M. (2010). Importance of ocean heat uptake efficacy to transient climate change. Journal of Climate, 23(9), 2333-2344.
26. Geoffroy, O., Saint-Martin, D., Olivié, D. J., Voldoire, A., Bellon, G., & Tytéca, S. (2013). Transient climate response in a two-layer energy-balance model. Part I: Analytical solution and parameter calibration using CMIP5 AOGCM experiments. Journal of climate, 26(6), 1841-1857.
27. Shatwell, P., Czaja, A., & Ferreira, D. (2020, May). On the suitability of two-layer energy-balance models for representing deep ocean heat uptake. In EGU General Assembly Conference Abstracts (p. 10120).
28. Boyd, S. (1993). Introduction to Signals & Systems. Course EE102, Stanford University.
29. Åström, K. J., & Eykhoff, P. (1971). System identification—a survey. Automatica, 7(2), 123-162.
30. Ljung, L. (1998). System identification (pp. 163-173). Birkhäuser Boston.
31. de Larminat, P., & Thomas, Y. (1975). Automatique des systèmes linéaires... Flammarion.
32. Söderström, T., & Stoica, P. (1989). System identification. Prentice-Hall International.
33. Young, P. (1981). Parameter estimation for continuous-time models—a survey. Automatica, 17(1), 23-39.
34. Pronzalo, L., & Walter, E. (1997). Identification of parametric models from experimental data. Springer, Berlin Wentzell PD, Andrews DT, Hamilton DC, Faber K, Kowalski BR (1997) Maximum likelihood principal component analysis. J Chemom, 11, 339366Wong.
35. Landau, I. D. (2001). Identification in closed loop: a powerful design tool (better design models, simpler controllers). Control Engineering Practice, 9(1), 51-65.
36. Loehle, C. (2009). A mathematical analysis of the divergence problem in dendroclimatology. Climatic Change, 94(3-4), 233-245.
37. D'Arrigo, R., Wilson, R., Liepert, B., & Cherubini, P. (2008). On the 'divergence problem'in northern forests: a review of the tree-ring evidence and possible causes. Global and planetary change, 60(3-4), 289-305.
38. de Larminat, P. (2016). Earth climate identification vs. anthropic global warming attribution. Annual Reviews in control, 42, 114-125.
39. Cheng, L., Abraham, J., Hausfather, Z., & Trenberth, K. E. (2019). How fast are the oceans warming?. Science, 363(6423), 128-129.
40. Myhre, G., Highwood, E. J., Shine, K. P., & Stordal, F. (1998). New estimates of radiative forcing due to well mixed greenhouse gases. Geophysical research letters, 25(14), 2715-

2718.
41. Schneider, S. H., & Moss, R. (1999). Uncertainties in the IPCC TAR: Recommendations to lead authors for more consistent assessment and reporting. Unpublished document.
42. Courtillot, V., Gallet, Y., Le Mouël, J. L., Fluteau, F., & Genevey, A. (2007). Are there connections between the Earth's magnetic field and climate?. Earth and Planetary Science Letters, 253(3-4), 328-339.
43. Svensmark, H., Enghoff, M. B., Shaviv, N. J., & Svensmark, J. (2017). Increased ionization supports growth of aerosols into cloud condensation nuclei. Nature communications, 8(1), 2199.
44. Svensmark, H., Svensmark, J., Enghoff, M. B., & Shaviv, N. J. (2021). Atmospheric ionization and cloud radiative forcing. Scientific Reports, 11(1), 19668.
45. Landscheidt, T. (2000). Solar wind near Earth: Indicator of variations in global temperature. In The Solar Cycle and Terrestrial Climate, Solar and Space weather (Vol. 463, p. 497).
46. Soon, W., Connolly, R., & Connolly, M. (2015). Re-evaluating the role of solar variability on Northern Hemisphere temperature trends since the 19th century. Earth-Science Reviews, 150, 409-452.
47. Egorova, T., Schmutz, W., Rozanov, E., Shapiro, A. I., Usoskin, I., Beer, J., ... & Peter, T. (2018). Revised historical solar irradiance forcing. Astronomy & Astrophysics, 615, A85.
48. Feulner, G. (2011). Are the most recent estimates for Maunder Minimum solar irradiance in agreement with temperature reconstructions?. Geophysical Research Letters, 38(16).
49. Reinhold, T., Shapiro, A. I., Solanki, S. K., Montet, B. T., Krivova, N. A., Cameron, R. H., & Amazo-Gómez, E. M. (2020). The Sun is less active than other solar-like stars. Science, 368(6490), 518-521.
50. Feldman, D. R., Collins, W. D., Gero, P. J., Torn, M. S., Mlawer, E. J., & Shippert, T. R. (2015). Observational determination of surface radiative forcing by CO2 from 2000 to 2010. Nature, 519(7543), 339-343.
51. Takemura, T., Tsushima, Y., Yokohata, T., Nozawa, T., Nagashima, T., & Nakajima, T. (2006). Time evolutions of various radiative forcings for the past 150 years estimated by a general circulation model. Geophysical research letters, 33(19).
52. De Larminat, P. (2014). Climate Change: Identification and Projections. John Wiley & Sons.
53. Caldeira, K., & Myhrvold, N. P. (2013). Projections of the pace of warming following an abrupt increase in atmospheric carbon dioxide concentration. Environmental Research Letters, 8(3), 034039.
54. Ball, W. T., Unruh, Y. C., Krivova, N. A., Solanki, S., Wenzler, T., Mortlock, D. J., & Jaffe, A. H. (2012). Reconstruction of total solar irradiance 1974–2009. Astronomy & Astrophysics, 541, A27.
55. Bony, S., Stevens, B., Held, I. H., Mitchell, J. F., Dufresne, J. L., Emanuel, K. A., ... & Senior, C. (2013). Carbon dioxide and climate: Perspectives on a scientific assessment. Climate science for serving society: Research, modeling and prediction priorities, 391-413.
56. Connolly, R., Soon, W., Connolly, M., Baliunas, S., Berglund, J., Butler, C. J., ... & Zhang, W. (2021). How much has the Sun influenced Northern Hemisphere temperature trends? An ongoing debate. Research in Astronomy and Astrophysics, 21(6), 131.
57. Flato, G., Marotzke, J., Abiodun, B., Braconnot, P., Chou, S. C., Collins, W., ... & Rummukainen, M. (2014). Evaluation of climate models. In Climate change 2013: the physical science basis. Contribution of Working Group I to the Fifth Assessment Report of the Intergovernmental Panel on Climate Change (pp. 741-866). Cambridge University Press.
58. Gao, C., Robock, A., & Ammann, C. (2008). Volcanic forcing of climate over the past 1500 years: An improved ice core-based index for climate models. Journal of Geophysical Research: Atmospheres, 113(D23).
59. Hansen, J., Sato, M. K. I., Ruedy, R., Nazarenko, L., Lacis, A., Schmidt, G. A., ... & Zhang, S. (2005). Efficacy of climate forcings. Journal of geophysical research: atmospheres, 110(D18).
60. Hasselmann, K. (1997). Multi-pattern fingerprint method for detection and attribution of climate change. Climate dynamics, 13, 601-611.
61. Hegerl, G. C., Hoegh-Guldberg, O., Casassa, G., Hoerling, M., Kovats, S., Parmesan, C., ... & Stott, P. (2010). Good practice guidance paper on detection and attribution related to anthropogenic climate change.
62. Hollis, C. J., Dunkley Jones, T., Anagnostou, E., Bijl, P. K., Cramwinckel, M. J., Cui, Y., ... & Lunt, D. J. (2019). The DeepMIP contribution to PMIP4: methodologies for selection, compilation and analysis of latest Paleocene and early Eocene climate proxy data, incorporating version 0.1 of the DeepMIP database. Geoscientific Model Development, 12(7), 3149-3206.
63. Change, I. C. (2013). The physical science basis. Contribution of working group I to the fifth assessment report of the intergovernmental panel on climate change, 1535, 2013.
64. Krivova, N. A., Vieira, L. E. A., & Solanki, S. K. (2010). Reconstruction of solar spectral irradiance since the Maunder minimum. Journal of Geophysical Research: Space Physics, 115(A12).
65. Myhre, G., Shindell, D., Bréon, F. M., Collins, W., Fuglestvedt, J., Huang, J., ... & Zhang, H. (2013). Climate change 2013: the physical science basis. Contribution of Working Group I to the Fifth Assessment Report of the Intergovernmental Panel on Climate Change.
66. Myhre, G., & Stordal, F. (1997). Role of spatial and temporal variations in the computation of radiative forcing and GWP. Journal of Geophysical Research: Atmospheres, 102(D10), 11181-11200.
67. Nicholls, Z. R., Meinshausen, M., Lewis, J., Gieseke, R., Dommenget, D., Dorheim, K., ... & Xie, Z. (2020). Reduced Complexity Model Intercomparison Project Phase

1: introduction and evaluation of global-mean temperature response. Geoscientific Model Development, 13(11), 5175-5190.
68. PAGES 2k Consortium. Continental-scale temperature variability during the past two millennia. Nature Geosci 6, 339–346 (2013).
69. Remmelzwaal, S. R., Sadekov, A. Y., Parkinson, I. J., Schmidt, D. N., Titelboim, D., Abramovich, S., ... & Middelburg, J. J. (2019). Post-depositional overprinting of chromium in foraminifera. Earth and Planetary Science Letters, 515, 100-111.
70. Ropelewski, CF et Jones, PD, (1987): Une extension de l'indice d'oscillation australe Tahiti-Darwin. Revue météorologique mensuelle 115, 2161-2165.
71. Sato, M., Hansen, J. E., McCormick, M. P., & Pollack, J. B. (1993). Stratospheric aerosol optical depths, 1850–1990. Journal of Geophysical Research: Atmospheres, 98(D12), 22987-22994.
72. Senior, C. A., & Mitchell, J. F. (2000). The time-dependence of climate sensitivity. Geophysical Research Letters, 27(17), 2685-2688.
73. Shapiro, A. I., Schmutz, W., Rozanov, E., Schoell, M., Haberreiter, M., Shapiro, A. V., & Nyeki, S. (2011). A new approach to the long-term reconstruction of the solar irradiance leads to large historical solar forcing. Astronomy & Astrophysics, 529, A67.